Atmospheric Research 288 (2023) 106719

Contents lists available at ScienceDirect

Atmospheric Research

journal homepage: www.elsevier.com/locate/atmosres

Snowfall events in the Cantabrian Mountains of northwestern Spain: WRF multiphysics ensemble assessment based on ground and multi-satellite observations

Adrián Melón-Nava [a], Andrés Merino [b,*], José Luis Sánchez [b], Javier Santos-González [a], Amelia Gómez-Villar [a], Eduardo García-Ortega [b]

[a] Universidad de León (ULE), Department of Geography and Geology, Campus de Vegazana, 24071 León, Spain
[b] Universidad de León (ULE), Atmospheric Physics Group (GFA), Environmental Institute, 24071 León, Spain

ARTICLE INFO

Keywords:
WRF model
Physics parameterizations
Snow precipitation
Cantabrian Mountains
Webcams

ABSTRACT

Snowfall in elevated areas of the mid-latitudes has a strong impact on infrastructure, freshwater availability, and the climate system. The Cantabrian Mountains of the northwestern Iberian Peninsula are very vulnerable to climate change because of their moderate altitudes, which limits their snowfall. Monitoring snow events is essential for the evaluation of weather and climate prediction models. However, measurement networks are scarce in mountainous areas and have great uncertainties because of blizzards. In this study, a multiphysics ensemble of the Weather Research and Forecasting (WRF) model was designed using three microphysics and two planetary boundary layer (PBL) schemes to simulate nine snowfall events in the Cantabrian Mountains during autumn and winter 2021–2022. The WRF was validated using several snow characteristics, such as liquid water equivalent, snow cover, and snow depth. Liquid water equivalent was evaluated using snow-gauge networks and satellite products in an assessment of snow cover. In addition, a monitoring network of webcams and snow poles was implemented, improving the low density of snow observations in the mountains. The results showed good model performance for detection of snow cover and slight overestimation of liquid water equivalent and snow thickness, which may have been caused by under-catchment that is generally an effect of wind on the measurement systems and by snow compaction, respectively. Morrison microphysics and Mellor-Yamada-Nakanishi-Niino (MYNN PBL) yielded better results for liquid water equivalent at higher altitudes and output greater snow cover. The results help determine the best configurations for snow modelling in the study area to develop future studies of the spatiotemporal patterns of snow distribution.

1. Introduction

Snowfall is one of the most frequent natural hazards at mid and high latitudes, having important effects on transportation and infrastructure (Scherrer et al., 2013). However, snow is also a major freshwater resource (Mankin et al., 2015; Pulliainen et al., 2020), accumulating during winter at high altitudes, to be used during summer for food production (Viviroli et al., 2020). In the current context of global warming, substantial reductions in snowmelt and ensuing runoff are expected, with shifts from snowfall to rainfall at increasingly higher elevations (Musselman et al., 2018). Snow cover also has important implications in the climate system, namely, the surface energy balance through its effect on land surface albedo, the partitioning of sensible and latent heat fluxes, near-surface atmospheric stability, and horizontal energy transport (Rudisill et al., 2021).

Monitoring and forecasting of snowfall events are of vital importance to minimize the associated risks and manage water resources. In terms of monitoring, surface measurement networks are usually sparse and irregularly distributed and, at mid-latitudes, snowfall tends to occur in mountainous areas. Snow measuring systems based on the quantification of precipitation must have heated systems, producing evaporation losses when precipitation is weak. In addition, strong winds decrease the snow collected in snow gauges when wind shields are not installed, causing losses of ~20%–50% (Grossi et al., 2017; Masuda et al., 2019; Rasmussen et al., 2012). Similar values have been found in the Cantabrian Mountains, where the underestimation of snow precipitation using

* Corresponding author.
E-mail address: andres.merino@unileon.es (A. Merino).

https://doi.org/10.1016/j.atmosres.2023.106719
Received 23 December 2022; Received in revised form 7 March 2023; Accepted 16 March 2023
Available online 18 March 2023

the Spanish Meteorological Agency (AEMET) network is similar to that in the Pyrenees, but less than those in other areas of the Iberian Peninsula (Buisán et al., 2017, 2022). The importance of location and wind exposure of precipitation measuring instruments has been highlighted in the Solid Precipitation Intercomparison Experiment of the World Meteorological Organization (Nitu et al., 2019).

There are major uncertainties in forecasting snow events. Snow and liquid precipitation are discontinuous variables that depend on complex microphysical processes at small scale that cannot be explicitly described, so we rely on parameterization. Moreover, in snow prediction, variations in melting level and multiple influences on deposition on the surface make prediction even more complex. The microphysics schemes include different ways to simulate hydrometeor classes and microphysical processes, and various assumptions are made regarding the size distribution (Molthan and Colle, 2012). The inclusion and treatment of ice hydrometeors improves the representation of convective events (Liu and Moncrieff, 2007; Adams-Selin et al., 2013) and differences in the parameterization of ice behaviour influence the accuracy of surface precipitation forecasts (Thompson et al., 2004). Also, surface heat fluxes parameterized by PBL schemes are important for severe weather events (Fernández-González et al., 2016). Therefore, the choice of parameterization scheme has a strong impact on simulations of phenomena such as snowfall and orographic and convective precipitation (Fernández-González et al., 2016; Miglietta et al., 2015; Bryan and Morrison, 2012).

The WRF model has been extensively used for snowfall event forecasting (Lee et al., 2022; Liu et al., 2018; Gerber et al., 2018). Additionally, WRF outputs have been implemented to force initial conditions in snow energy-balance models (Corripio and López-Moreno, 2017; Alonso-González et al., 2018, 2021; Raparelli et al., 2023).

Several studies have assessed the sensitivity of WRF to parameterization schemes for snowfall events. Results have varied with the study area, validation databases, and variables used for the evaluation. Comin et al. (2018) observed a strong variability among WRF results, evidencing the critical role of microphysics in extreme snowfall events of the Southern Andes. Similar conclusions were reached by simulating snowfall events over Antarctica (Vignon Besic et al., 2019). McMillen and James Steenburgh (2015) used WRF to examine the sensitivity of simulations for the Great Salt Lake lake–effect snowstorm to the microphysics parameterization. The results showed better estimation of precipitation with Thompson scheme and overprediction with Goddard and Morrison for the estimation of radar-based liquid equivalent precipitation. Fernández-González et al. (2015) evaluated WRF for snowfall episodes on the northwestern Iberian Peninsula based on snow water equivalent. The results showed an overestimation of all schemes, with the Thompson microphysics and Mellor-Yamada-Janjic (MYJ) PBL parameterizations providing the best results. Ghafarian (2021) also highlighted the overestimation of snow liquid equivalent by WRF, although he disagreed with the microphysics scheme selected by Fernández-González et al. (2015). Agreement on the overestimation of snow water equivalent by WRF and discrepancies among the microphysics schemes may be attributed to the data. Thus, studying an extraordinary snowfall event on the Iberian Peninsula, Buisán et al. (2022) found that measurements from the AEMET operational rain-gauge network underestimated solid precipitation by 20%–30%. The fundamental reason was a combination of heavy precipitation, cold temperatures and winds, phenomena that usually occur at high altitudes. The present study highlights the difficulty of evaluating prediction models for snowfall events based exclusively on snow liquid equivalent. For this reason, it is advisable to focus on model evaluations using other snow characteristics such as snow cover and depth. However, the lack of available databases on these variables has made the number of studies scarce.

Snow cover and depth are valuable data on snow properties. The main methods for monitoring these are in situ measurements and satellite remote sensing (Portenier et al., 2020). Ground-based monitoring networks are often integrated with webcam networks (Piazzi et al., 2019; Tanis et al., 2020; Arslan et al., 2017). The analysis of webcam images allows detailed monitoring of snow properties, such as snow cover fraction, thickness, and snow cover redistribution at very high temporal resolution, which is one of its main advantages (Bongio et al., 2021). Additionally, remote sensing data from satellites provide information on a regional scale. To solve limitations caused by clouds, products combining reflective, passive, and active microwave data are considered the best choice for snow monitoring (Dietz et al., 2012). Moreover, the use of satellites facilitates the study of snow in inaccessible areas.

The Cantabrian Mountains on the northwestern Iberian Peninsula (Fig. 1) receive frequent snowfall during winter. However, in recent decades, they have had negative trends in winter precipitation and positive trends in average temperatures. These trends are expected to continue in the coming decades, which could spell significant reductions in snowfall and thus a reduced duration of snow cover because of an increase in melting level (Merino et al., 2014). Furthermore, several studies agree that the Cantabrian Mountains will be the Iberian Peninsula mountain system most affected by climate change regarding declines in snow resources (Merino et al., 2014; Alonso-González et al., 2020; Pons et al., 2010; Lastrada et al., 2021), affecting the number of snow days, duration of snow reserves, and volume of precipitation. This would thereby affect water resources in the Cantabrian Mountains, owing to the regulating effect of snow resources on river flows and floods (Pisabarro et al., 2019). Shorter durations and less snow accumulation are expected, which could reduce average flows in the coming decades, combined with increases in peak snowmelt flows because of rising temperatures (Lastrada et al., 2021). Although exceptional snowfalls are infrequent, such events cause severe damage. Heavy or long-lasting snowfalls are usually aggravated by strong winds, which accumulate several metres of snow in inhabited areas, generating long-lasting snow patches (Santos-González et al., 2010b). As a result, there are frequent communication difficulties, infrastructure damage, or avalanches. These have caused fatalities in recent years, indicating a natural hazard (Beato-Bergua et al., 2019; García-Hernández et al., 2018; González Trueba and Serrano Cañadas, 2010; Santos-González et al., 2010a). These also damage forests during early, late, or extraordinary snowfalls (Nykänen et al., 1997). Snow also has implications for geomorphological processes and the surface thermal regime (Gallinar-Cañedo et al., 2022; Pisabarro et al., 2017; Melón-Nava et al., 2022), and so is of great geo-ecological relevance.

The main objective of the present work is to evaluate a multiphysics ensemble of the WRF model for snowfall events. For this purpose, we examined nine snowfall events in the Cantabrian Mountains during the 2021/2022 cold season (November–February) plus three microphysics and two PBL parameterizations. Validation was performed based on snow water equivalent, snow cover and depth, using observational networks and satellite products.

The paper is structured as follows: the study area and databases are described in section 2; Section 3 presents the methodology; principal results are given in section 4; a discussion and conclusions are provided in section 5.

2. Study area and database

The Cantabrian Mountains of the northwestern Iberian Peninsula extend from west to east for about 300 km. The highest areas are above 2000 m a.s.l., with the greatest altitudes in the Picos de Europa, where several peaks exceed 2600 m a.s.l. It is an area with marked asymmetry between slopes and sectors, which creates a variety of climates (Serrano et al., 2015). The range is characterised by a longitudinal arrangement of the highest altitudes, forming a divide nearly parallel to the Cantabrian coastline. This generates great differences in snowfall between mountain sectors, strongly influenced by altitude or orographic barriers (Allende Alvarez, 2008; Ortega-Villazán and Morales-Rodríguez, 2015).

The average annual temperature over 1981–2010 varied between 5

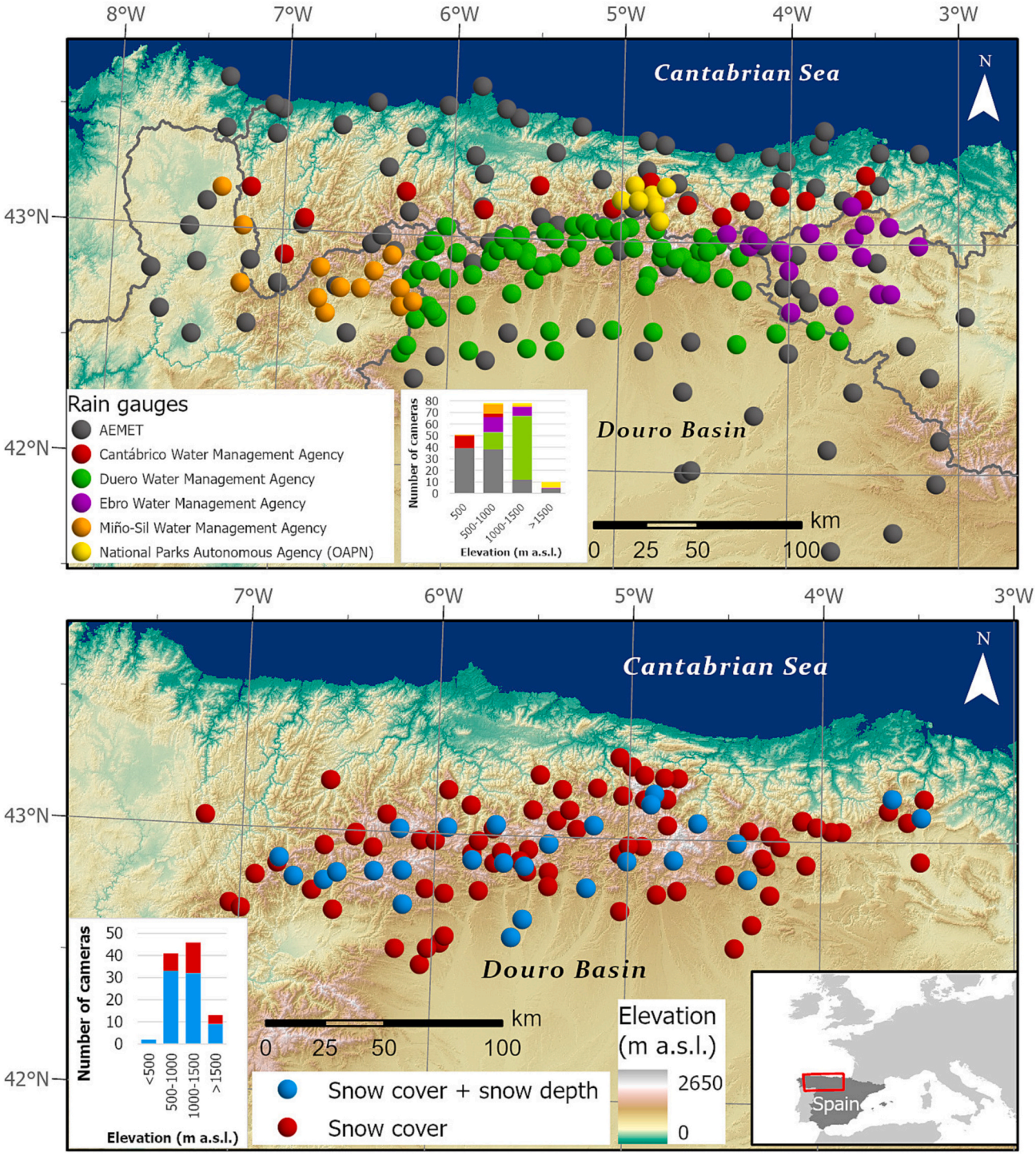

Fig. 1. Topographic map of Cantabrian Mountains. Points form the rain and snow station network.

and 10 °C, although the average temperature during winter was negative in a large part of the study area. Mean annual precipitation varied between 800 and > 2000 mm (AEMET, 2011) with marked asymmetry, including heavier amounts on the northern slope and at the eastern and western ends. The mean number of snow days has been estimated at 15 to >60 days (Ortega-Villazán and Morales-Rodríguez, 2015), with larger numbers at the higher altitudes of the main divide. The study area is classified in Köppen-Geigen as Cfb, Dsc, and Dfc (Chazarra-Bernabé et al., 2022).

Precipitation during snowfall episodes has been evaluated using snow gauges (Fig. 1) from AEMET, water management agencies, and the Global Change Monitoring Network in national parks. These agencies use different snow-gauge sensors with variable temporal resolutions (Table 1). Quality control and homogeneity has been checked and hourly aggregates have been calculated for all station data.

Snow cover and thickness were validated using a monitoring network consisting of webcams and snow poles. Fifteen *Wi*-Fi webcams and four time-lapse cameras were installed, which, together with other public webcams, made a total of 105 snow-cover observations in an altitudinal range of 200–2100 m a.s.l. (Fig. 1). For snow thickness observations, 27 sites were used. For this purpose, cameras were complemented by snow poles (Fig. 2), consisting of vertical stakes with

Table 1
Snow gauge characteristics.

Data source	Number of gauges	Resolution (minutes)	Altitudinal range (m)
AEMET	92	10	0–1700
Cantábrico Water Management Agency	17	60	100–900
Duero Water Management Agency	70	10	700–1500
Ebro Water Management Agency	20	15	500–1700
Miño-Sil Water Management Agency	15	60	400–1200
National Parks Autonomous Agency (OAPN)	8	10	700–2400
Total	222		0–2400

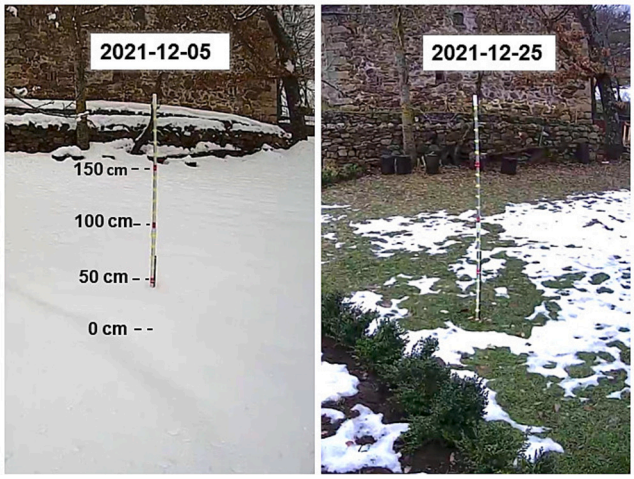

Fig. 2. Snow-depth measurement at Santa María de Redondo - Palencia (42.9903°N, −4.4374°W, 1204 m a.s.l.) on 5 and 25 December 2021.

graduated reflective marks every 10 cm. This allows the recording of thicknesses up to 2 m for monitoring snow cover, even at night.

A massive semi-automatic download of screenshots was done every 6 h, yielding 4 observations per day of both snow cover and thickness. Subsequently, the images were manually recorded in a database. The maximum daily value of cover and thickness was recorded. There were sites with light snowfalls, covering the ground for only a few hours, followed by rapid melt periods. The main advantage of this method is the ability to acquire simultaneous data, even at remote locations, as evaluated in Bongio et al. (2021). This allows the creation of time series of snow cover and thickness, which were used as validation data in our work as an alternative to a non-existent network for monitoring snow in the Cantabrian Mountains. These data have sufficient temporal resolution to detect rapid changes and provide detailed information on snow dynamics at the sampling locations. However, they have some limitations, notably an intermittent loss of connection at some sites, which can last several days. Another common problem is blinding of the camera lens due to compaction of snowflakes on it, leading to missing data during blizzards.

Satellite observations were obtained from the "IMS Daily Northern Hemisphere Snow and Ice Analysis, 1 km". This product is derived from the Interactive Multisensor Snow and Ice Mapping System (IMS) and is now available from the third version from the National Oceanic and Atmospheric Administration / National Environmental Satellite, Data, and Information Service (Ramsay, 1998; Helfrich et al., 2007). There has been improvement of the IMS-NOAA product since 1997 (Helfrich et al., 2007), with a reduction in pixel resolution from 24 to 1 km. This has allowed a daily product to be derived from satellite (POES/GOES) and microwave products (DMSP and AMSR-E) and synthetic aperture radar imagery. The product distinguishes snow cover using active microwave data, which facilitates data collection even during cloud cover and nighttime, strongly differentiating it from passive satellite products. IMS provides daily layers classified into four values: open water, snow-free land, sea or lake ice, and snow-covered land. The last was of interest in our study. IMS has been compared to other satellite platforms such as MODIS (Brubaker et al., 2005; Li et al., 2019), obtaining seasonally variable results. There was better accuracy during winter than autumn and spring. Other studies have highlighted that the largest differences in snow detection between IMS and MODIS are in the snow ablation season (Frei and Lee, 2010). In the present study, we did not use MODIS as a validation tool for snow cover because of substantial cloud cover during the nine snowfall events analysed. IMS has been compared with reanalysis products, which tend to overestimate snow depth and cover (Orsolini et al., 2019). The latter authors showed that accuracies of snow detection between in-situ observations and IMS reached 90% in their study of the Tibetan Plateau, values similar to those from a comparison of IMS-NOAA with ground-based measurements over the continental USA (Chen et al., 2012).

3. Methodology

Nine study cases during autumn and winter 2021/2022 (Fig. 4) were selected, based on snow depth and cover recorded by the observation network described in Section 2. Once the case studies were chosen, a multiphysics ensemble was developed using the non-hydrostatic Advanced Research WRF model version 4.1 (Skamarock and Klemp, 2008). Simulations were run using the National Centers for Environmental Prediction Global Forecast System analyses with 0.25° horizontal grid spacing as initial and boundary conditions. Thus, using a two-way nesting strategy, two nested domains with spatial resolutions 9 and 3 km were created (Fig. 3). Vertical resolution was set to 54 levels for both domains. For each case study, 30-h simulations were executed, leaving six hours of the previous day as the spin-up period.

Physical parameterizations are an essential part of numerical weather prediction models because there are processes, such as turbulence, convection and microphysics, that occur at subgrid scale. To test the influence of parameterizations on several snow precipitation characteristics of WRF, a multiphysics ensemble was constructed from three microphysics and two PBL schemes (Table 2). The selected microphysics schemes were: (I) Goddard one-moment bulk microphysical (Tao et al., 2016); (II) new Thompson (Thompson et al., 2008); (III) new bulk microphysics Morrison and Milbrandt (Milbrandt and Morrison, 2016).

The Goddard scheme includes the resolution of four ice classes: cloud ice, snow, graupel, and frozen drops/hail. The scheme has substantial modifications over the earlier three ice classes (Tao et al., 2009), including allowances for supersaturations >20%, mitigation of spurious evaporation/sublimation, a bin microphysics following the specifications of Li et al. (2009a, 2009b, 2010), rain evaporation correction but with physical raindrop size constraints, and a vapor diffusivity factor. The snow/graupel size-mapping schemes were adjusted to obtain greater stability at larger mixing ratios and increase the aggregation effect for snow. A snow density map was also added (Brandes et al., 2007).

The Thompson scheme assumes that the size distribution of snow particles is dependent on both liquid water content and temperature. In addition, the scheme incorporates realistic characteristics of snow particles, such as their nonspherical shape and a bulk density that varies

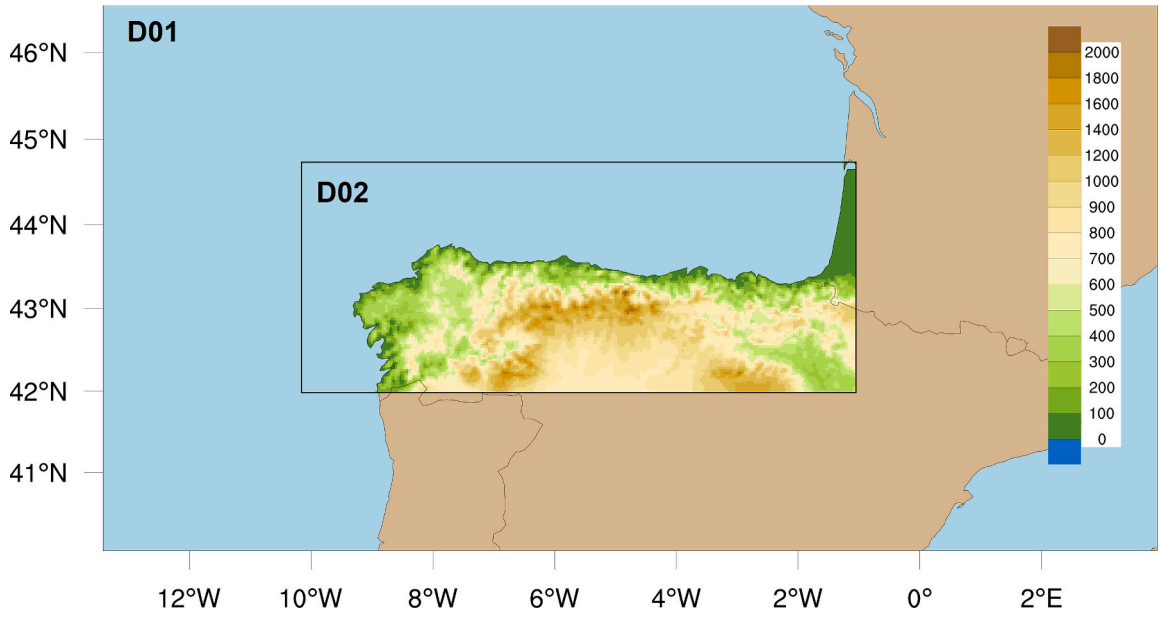

Fig. 3. WRF Domains.

Table 2
WRF multiphysics ensemble.

Physical parametrization		Reference	Ensemble number					
			WRF1	WRF2	WRF3	WRF4	WRF5	WRF6
Multiphysics	Goddard one-moment bulk microphysical scheme	Tao et al. (2016)	X	X				
	New Thompson scheme	Thompson et al. (2008)			X	X		
	New bulk microphysics Morrison and Milbrandt scheme	Milbrandt and Morrison (2016)					X	X
PBL	YSU: Yonsei University Scheme	Hong et al. (2006)	X		X		X	
	MYNN: Mellor–Yamada Nakanishi Niino	Nakanishi and Niino (2006); Olson et al. (2019)		X		X		X

inversely with diameter (Heymsfield et al., 2007). Another important new feature of the scheme pertains to snow accreting cloud droplets, or riming. Instead of considering a constant collection efficiency of 100%, the efficiency is calculated based on the average volume diameter of snow and cloud water according to Wang and Ji (2000).

The new Morrison and Milbrandt scheme advances a modified version of predicted particle properties, including multiple free ice-phase categories. This is in contrast to the previous scheme that included a single ice-phase category with four prognostic mixing ratio variables, i.e., total ice mass, ice number, ice mass from rime growth, and bulk rime volume (Morrison and Milbrandt, 2015). This modification removes the limitation that only allowed for populations of one type of ice particle to exist at a given point in time and space.

The selected PBL schemes were (I) Yonsei University (YSU; Hong et al., 2006) and (II) Mellor–Yamada Nakanishi Niino (MYNN; Nakanishi and Niino, 2006; Olson et al., 2019).

The YSU PBL improves on previous versions proposed by Noh et al. (2003) by including an explicit treatment of entrainment processes at the PBL top. The scheme was incorporated into WRF, producing a realistic structure of the PBL, improving representation of the mixing layer in convective and frontal situations.

MYNN introduces a new turbulent kinetic energy PBL. The new scheme has been shown superior to preceding Mellor-Yamada-type PBL schemes (Mellor and Yamada, 1974, 1982) in simulating the PBL convective layer. In addition, it introduces improvements in the representation of nonlocal mixing, interaction with clouds, and coupling with other model components in WRF.

Based on the results of other studies, the following schemes were selected: Dudhia (1989) for shortwave radiation; Rapid Radiative Transfer Model (Mlawer et al., 1997) for longwave radiation; Eta surface layer described by Janjić (1994) and Noah Land Surface Model (Chen and Dudhia, 2001); Kain-Fritsch cumulus scheme (Kain, 2004) with explicit resolution of cumulus in the inner domain.

Once the WRF simulation ensemble was designed, we developed a method for the validation of snow precipitation. The ensemble members were initialised with the same atmospheric conditions and thus had the same probability of producing the most accurate result (Schwartz et al., 2010). The validation was done using density plots and statistical goodness-of-fit measures, focusing on three event characteristics, namely, 24-h accumulated liquid water equivalent (LWE), maximum snow cover, and maximum snow depth. LWE was chosen because measurement systems do not discriminate precipitation type and variations of melting level throughout an event cause recorded precipitation to be a mixture of rain and snow at some stations. The ensemble was validated pixel-to-point to avoid interpolations of precipitation, which has strong spatial variability, and LWE was evaluated by elevation range.

A density plot is a smoothed version of the histogram that allows global comparison of recorded and modelled precipitation amounts (Fig. 4). Visual comparison of the distribution is complemented by adding the D statistic from the Kolmogorov-Smirnov (K—S) test as a measure of deviation between the two distributions. That test measures the maximum difference between observed and modelled cumulative distributions. The K—S distance statistic and its *p*-value were computed. The null hypothesis assumes that both samples come from a population with the same distribution. When that hypothesis can be rejected with

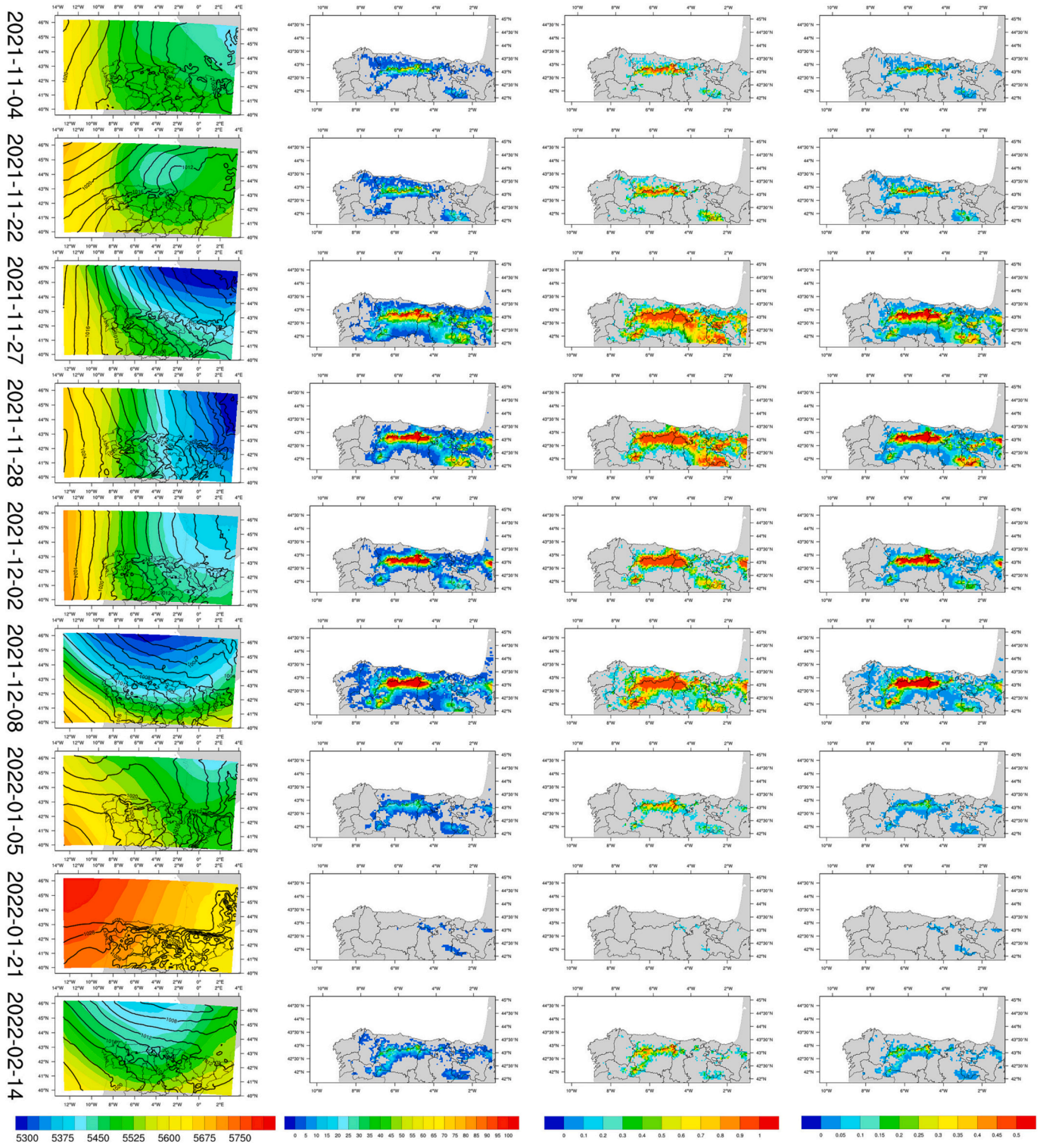

Fig. 4. Selected study cases. First column: sea level pressure (hPa, lines) and geopotential height at 500 hPa (gpm, shadow). Second column: 24-h accumulated snow water equivalent (mm). Third column: maximum snow cover (%). Fourth column: maximum snow depth (m).

significance, there is a significant difference between the distribution of the two samples.

Scatter plots were used for pairwise comparison of modelled and observed data (Fig. 5). The data fit was evaluated using the modified Kling-Gupta efficiency (KGE; Gupta et al., 2009, Kling et al., 2012). This index compares observed and modelled precipitation based on three components, linear correlation (r), bias ratio (β), and variability ratio (γ). r is the Pearson product-moment correlation coefficient, β reflects total precipitation compared to ground-based observations, indicating the average tendency of the gridded precipitation to underestimate ($\beta < 1$) or overestimate ($\beta > 1$), and γ measures relative dispersion between the gridded and ground-based measurements. The optimal value for KGE and all its components is one. This index has been widely used to evaluate model performance for precipitation (e.g., Somos-Valenzuela and Manquehual-Cheuque, 2020; Merino et al., 2021).

Snow cover was first validated as binary, i.e., absence or presence.

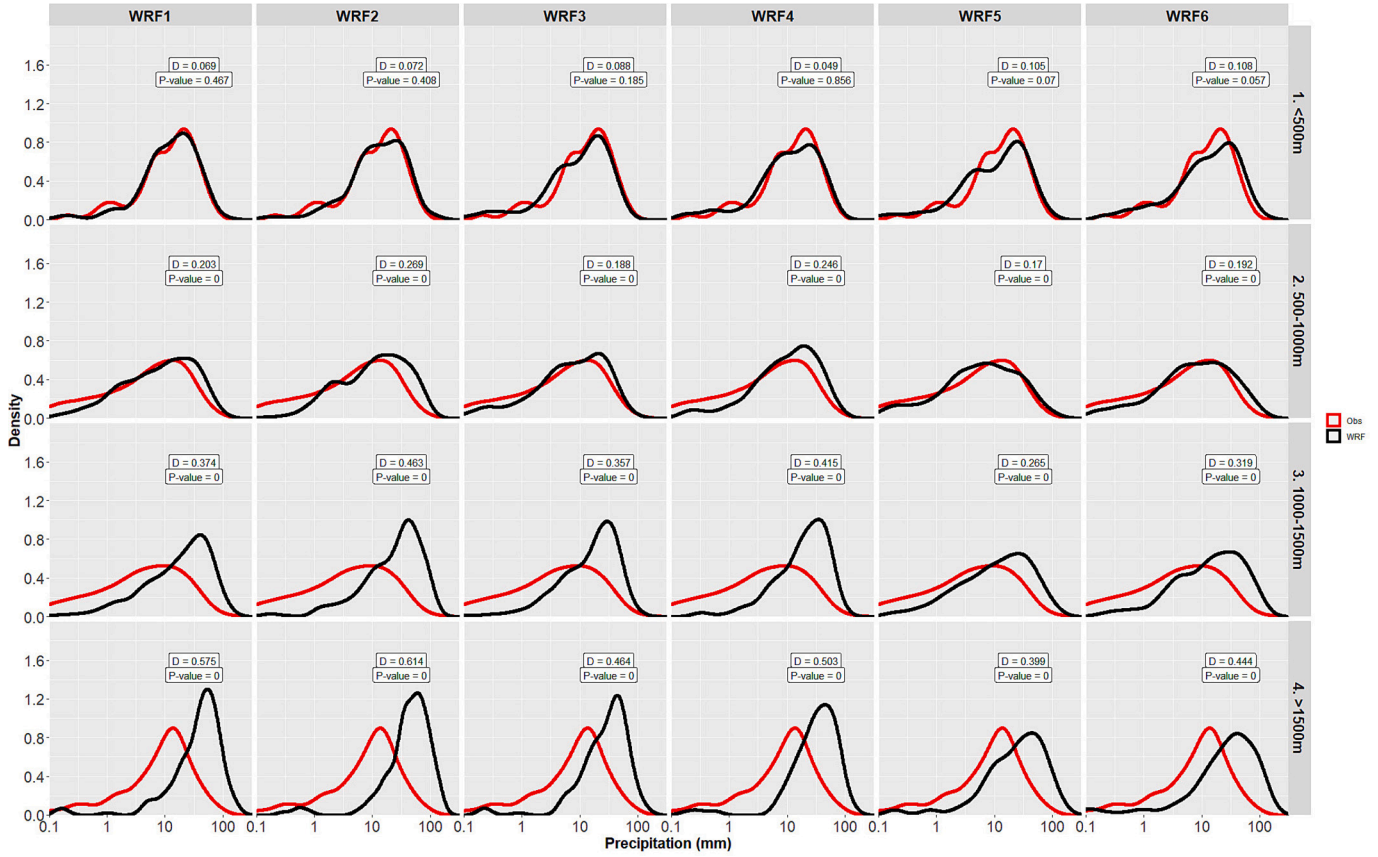

Fig. 5. Density plots for observed daily precipitation distribution (red line) vs. WRF precipitation (black line). Rows show different altitude ranges and columns the WRF combinations. (For interpretation of the references to colour in this figure legend, the reader is referred to the web version of this article.)

The results were presented based on various skill scores such as probability of detection (POD), false alarm rate (FAR), and critical success index (CSI). In contrast, the IMS data were re-gridded to the WRF domain to grid and the number of pixels of coincidence or discrepancy with WRF snow cover was calculated.

Finally, snow depth was evaluated using the snow-pole network, extracting maximum daily thickness. Average BIAS, MAE and RMSE were calculated for each case study and ensemble member. The indexes were each standardized by dividing by daily averages.

4. Results

This section first analyses the characteristics of the case studies and then describes the results of the validations of the ensemble designed with WRF. The model was validated based on characteristics of the snowfall events, namely, total accumulated precipitation (rain and snow), snow cover, and snow depth.

4.1. Snow event features

First, the synoptic environments of the snowfall events of winter 2021/2022 were described and the ensemble means for snow water equivalent, snow cover and depth were extracted (Fig. 4). Synoptic settings of the snow days in the Cantabrian Mountains included northerly advection (2021-11-04; 2021-11-27; 2021-11-28; 2021-12-02), prevailing shifts to northwesterly (2022-02-14; 2021-12-08) or northeasterly (2021−11−22). At mid-levels, there were troughs to the northeast of the Iberian Peninsula, with the Cantabrian Mountains to the east of the trough, producing meridional flows. These events are representative of the favourable conditions for snowfall in the mountains. These conditions are: a moist northerly flow (owing to its interaction with the Cantabrian Sea) that impacts the mountains perpendicularly; a strong isobaric gradient in mid and low layers, which favours the displacement of precipitation to southern slopes; cold air in mid-layers, which creates thermal instability. Thus, in the study cases with the strongest isobaric gradient (2021-11-27; 2021-11-28; 2021-12-02), maximum precipitation and snow depth was observed on southern slopes. In contrast, in the cases with a weaker isobaric gradient (2021-11-22; 2022-01-21), precipitation concentrated on the north faces, with the most intense snowfalls near the watershed. Other synoptic situations favourable for snowfall in the Cantabrian Mountains, such as air mass collisions, were not observed during the 2021–2022 study period.

Eight of the nine winter snowfall events affected the entire mountain range. One (2022-01-21) affected only the eastern part of the range, since it occurred in an environment of high sea-level pressure and weak northeast flow at upper levels.

4.2. Liquid water equivalent validation

Liquid water equivalent is the main variable to assess the performance of model precipitation, without distinction between solid and liquid phase. Fig. 5 shows a density plot with the simulated and observed accumulated precipitation as a function of WRF configuration and station elevation. Thus, altitude is an important factor in the results because the melting level was ~500 m a.s.l. during the events. A similarity of simulated and observed precipitation distributions for stations with altitudes <500 m a.s.l. should be highlighted. For all models, there were no significant differences between the distributions (p-value >0.05). However, the differences increased with station elevation, with greater discrepancies for stations >1500 m a.s.l., with a significant underestimation of precipitation. Regarding the WRF configurations, WRF5 gave better results for all elevations (smaller D statistic), except

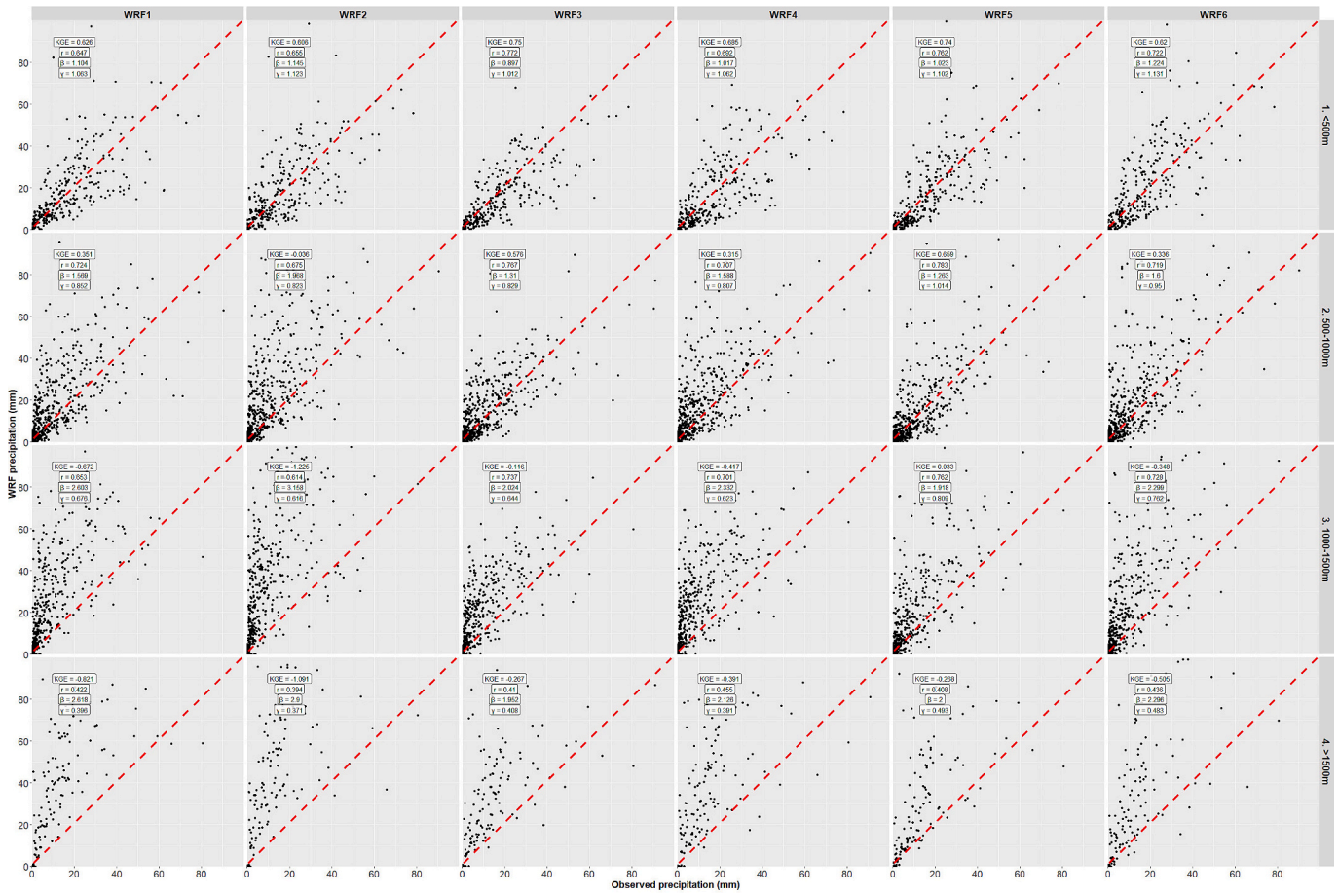

Fig. 6. Scatter plots of observed daily precipitation vs. WRF precipitation. Rows show altitude ranges and columns WRF combinations. Perfect fit shown by red dashed line. (For interpretation of the references to colour in this figure legend, the reader is referred to the web version of this article.)

<500 m a.s.l., where WRF4 showed better performance. YSU PBL obtained better results for higher elevations and microphysics and Morrison microphysics was superior at elevations above 500 m a.s.l. where the precipitation was solid.

Similar results are seen in Fig. 6, where scatter plots show predicted and observed accumulated precipitation as a function of WRF configuration and station elevation. Elevation remained the main factor, with poorer performance by all models in terms of correlation (r), bias (β) and variability (γ) as altitude increased. The overestimation of precipitation by the model increased with elevation ($\beta > 0$). Surprisingly, PBL parameterizations were just as important as microphysics for precipitation performance. The best performance of the KGE and parameters is seen for WRF3 and WRF5, concurring again with Morrison and YSU PBL. MYNN PBL gave superior results only for stations >1500 m a.s.l. Liquid water equivalent verification was completed using a Taylor diagram (Fig. 7). The results show tiny differences between ensemble members for stations at similar elevations in terms of the correlation coefficient, with greater differences in standard deviation and root-mean-square difference (RMSD). The largest differences again appear to be a function of station altitude. The correlation coefficients decrease smoothly for high-altitude stations, with marked declines at >1500 m a.s.l. However, RMSE and standard deviation are similar for all altitudes, except for stations 1000–1500 m a.s.l. Thompson microphysics produced the smallest RMSD, whereas Goddard had the worst performance. However, the PBL parameterization had a prominent role, with YSU PBL clearly superior to MYNN PBL for all microphysics parameterizations and altitudes.

4.3. Snow cover validation

Depending on surface temperature, snow particles can melt on contact with surfaces or accumulate in the solid phase. Snow accumulation on surfaces can cause major problems for human activities. For this reason, a snow-cover forecast provides valuable information beyond snow precipitation. Good model performance for snow cover depended not only on the precipitation forecast but on surface temperature and the precipitation phase. Fig. 8 shows CSI, FAR and POD verification scores by day and WRF combination. As expected, days with very extensive snowfall (i.e., 2021-11-27) had the best results in terms of high POD, low FAR, and therefore high CSI. On these days, most stations monitoring snow cover reported 100% cover and all WRF members effectively simulated this. On the contrary, on the days when snow cover was limited to the highest stations (i.e., 2022-02-14) the members producing a higher POD (WRF2 and WRF4) also gave a higher FAR. This behaviour is typical in binary validations. In the validation for all events, there were no substantial differences between ensemble members. The WRF4 yielded the highest CSI and POD but also the highest FAR. In contrast, the WRF5 output the smallest values for all verification scores. Thus, Morrison microphysics and YSU PBL posted the best performance, as in the liquid water equivalent validation.

Given the limited number of stations with snow-cover monitoring, it was decided to use products derived from meteorological satellites. Cloudiness was nearly continuous during the snow events in the Cantabrian Mountains, so visible and infrared sensors could not detect surface characteristics. Consequently, the choice of sensors with the ability for surface monitoring under cloudiness is critical. Fig. 9 shows the maximum snow-covered area in the IMS satellite product vs. that

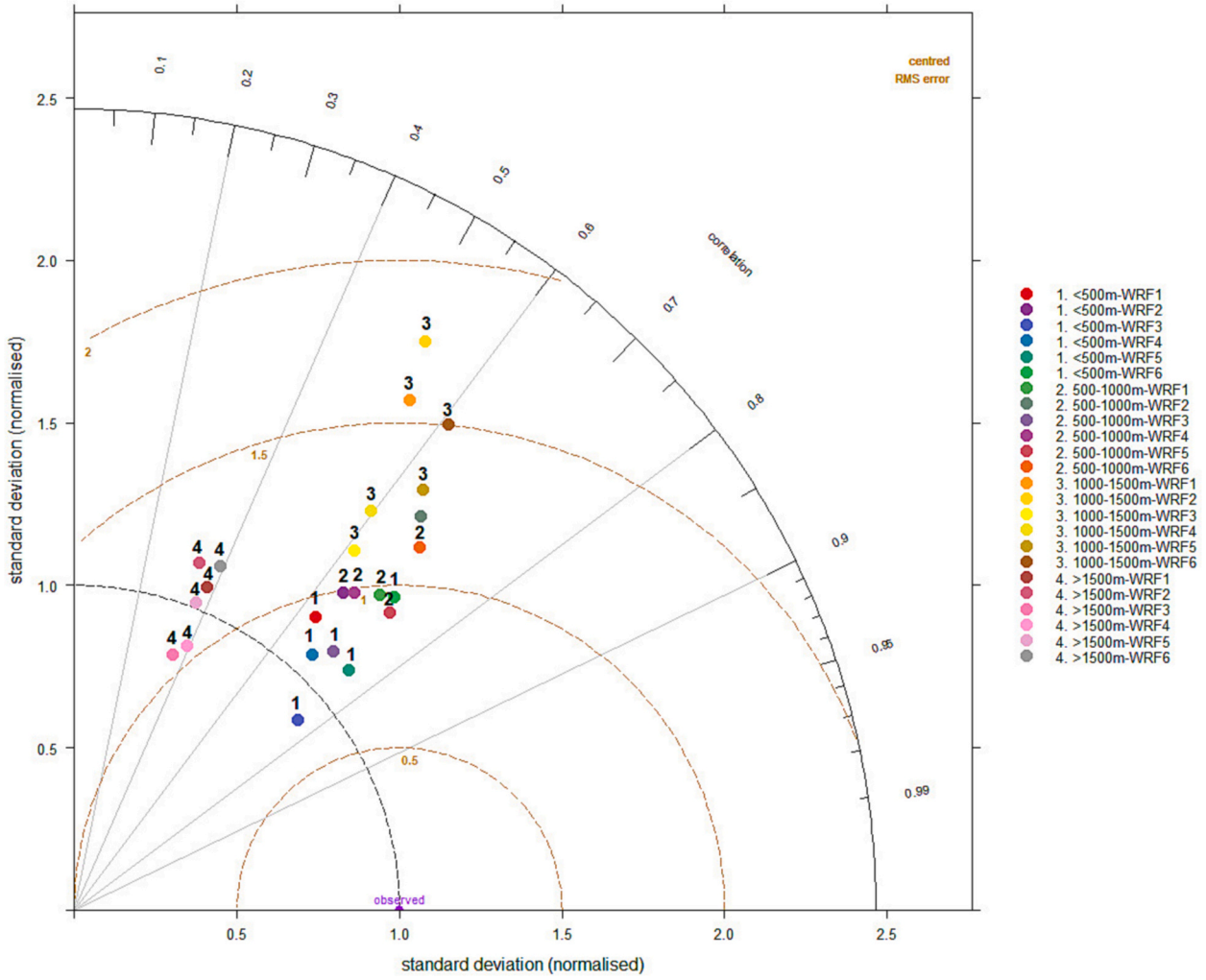

Fig. 7. Taylor diagram showing correlation coefficient, RMSD, and standard deviation resulting from different settings of WRF model and altitude ranges.

predicted by the model for each event. The green colour represents areas where the WRF and satellite data agree on snow cover. Yellow areas show where only the model forecast snow cover and orange where only the satellite detected it. The results show strong variability. There were events with greater snow cover predicted by the model relative to that observed by satellite (i.e., 2021-11-27 and 2022-02-14), and the reverse (i.e., 2021-11-22 and 2021-12-08). Regarding the WRF configurations, MYNN PBL tended toward greater snow cover compared to YSU PBL, because the former forecast a slightly lower melting level. Regarding the microphysics schemes, the same behaviour was observed in all cases. Goddard microphysics (WRF1 and WRF2) predicted a smaller snow cover extent, whereas Morrison microphysics (WRF5 and WRF6) gave the greatest snow cover. Thus, for events in which the WRF predicted a higher melting level than observed (i.e., 2021-11-22), Morrison yielded better overall results. However, when the WRF underestimated the melting level (i.e., 2021-11-04 and 2022-02-14), Goddard was superior. These results can be related to atmospheric conditions during the events (Fig. 3). For days with northerly advection (i.e., 2021-11-28 and 2021-12-02), the models were very consistent with the observations. With northwesterly advection (i.e., 2021-11-27 and 2021-12-08), the model tended to overestimate snow cover, and with northeasterly advection (i.e., 2021-11-22 and 2022-01-21), there was underestimation.

Finally, snow cover detection was evaluated for WRF configurations and snowfall events based on 2628 webcam images. This resulted in 78.12% hits in terms of presence or absence of snow cover, 19.02% false negatives (snow cover detected by the camera images but not by WRF), and 2.86% false positives (snow cover overestimated by WRF). The same analysis for observed snow depth revealed slight differences between WRF configuration. Overall, hit rates for snow cover ~70% were calculated in areas with thicknesses 0–10 cm, with ~80% for thicknesses 10–30 cm and ~ 100% for thicknesses >30 cm, a threshold at which the false negatives disappeared.

4.4. Snow depth validation

Snow depth is perhaps the best indicator of snowfall intensity, but its monitoring presents major challenges. The depth depends not only on the amount of snow precipitation but also on compaction or wind transport, which can greatly modulate thickness of the snow layer. Snow depth is therefore one of the most complex variables to simulate, and validation results were strongly dependent on wind exposure in the measurement area. For this reason, the location of measurement is critical to be representative of the surrounding area. In our study, the measurements were taken in flat areas, avoiding locations exposed to wind or gust. The selected events showed strong variability of snow depth measured with the snow-pole network. The greatest snow depth was recorded on 2021-11-28, with a maximum thickness of 130 cm and average 45 cm. Conversely, on 2021-11-04 and 2022-01-21, thicknesses barely exceeded 10 cm and very few sampling points were affected.

Figure 10 shows results of the quantitative snow depth validation in terms of BIAS, MAE and RMSE. There was general overestimation of snow depth in all cases and WRF configurations, although the models

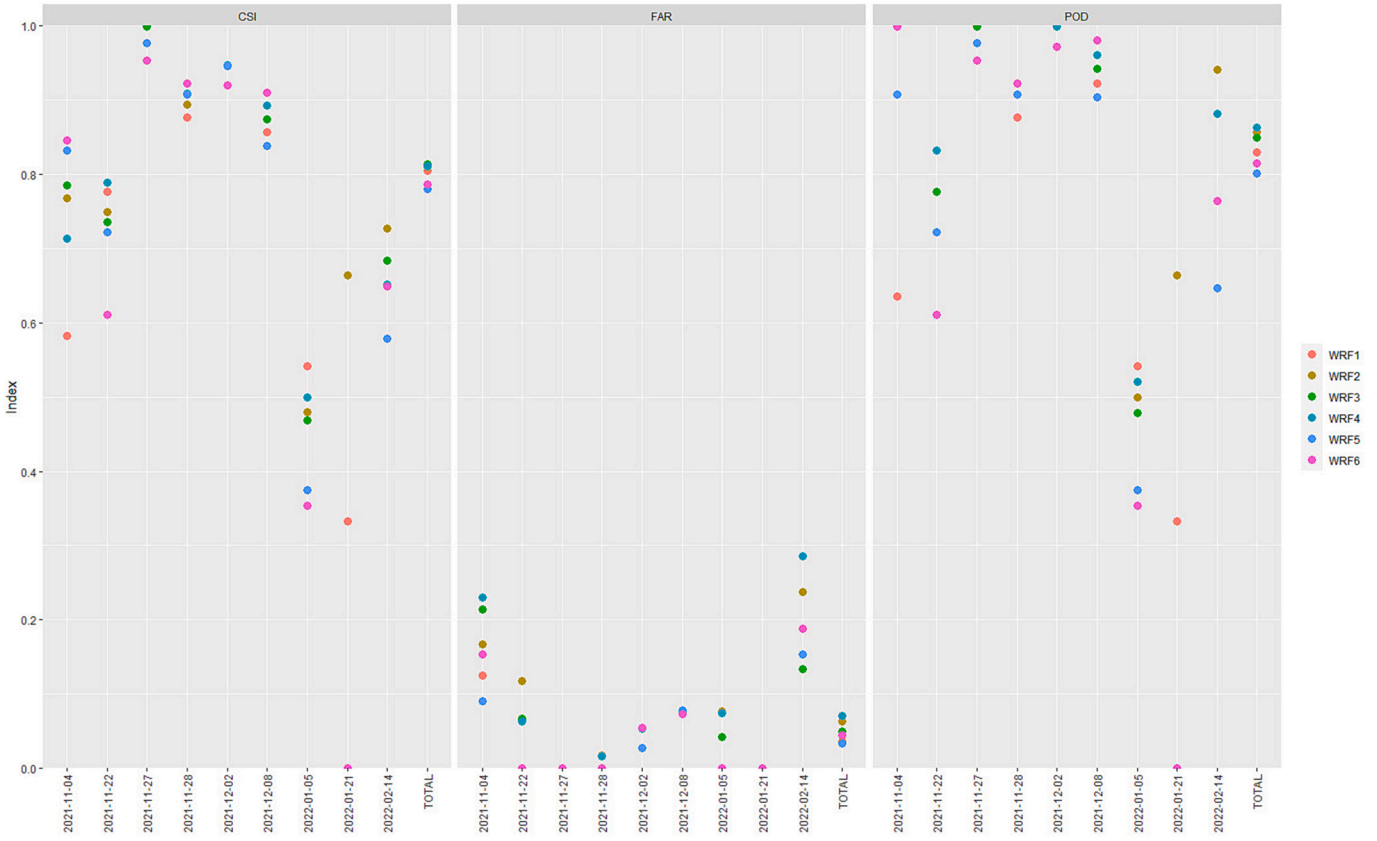

Fig. 8. Snow cover verification scores by day and WRF combination.

effectively captured the observed thickness variability between events. The good fit of the models on 2021-11-28 is noteworthy because it was the event with the greatest recorded snow thicknesses. Events with small snow depths yielded more uneven results. Regarding the WRF configurations, Goddard microphysics showed the best behaviour for all indices, whereas Thompson microphysics had the greatest overestimation. Despite the importance of PBL parameterizations for liquid water equivalent and snow cover forecasts, the PBL settings had less impact on model thickness.

5. Discussion and conclusions

Snowfall prediction is a principal management tool in various fields like road safety, winter sport activities, avalanche risk assessment, and hydrology (Blanchet and Davison, 2011; Scherrer et al., 2013). In recent years, works have determined the models that can improve such prediction (Fernández-González et al., 2015; Hammer, 2018; He et al., 2016). This makes it essential to validate the models using observations. However, one of the main handicaps in validation is the availability of observational databases. On the Iberian Peninsula, snow falls mainly in the mountains, where precipitation measurement networks are scarce and there is greater spatial variability of precipitation. Moreover, because of demographic, geomorphological and economic reasons, measurements of snow precipitation have been especially scarce in the Cantabrian Mountains. This is even though the mountains have the heaviest winter precipitation on the peninsula (Lastrada et al., 2021). Moreover, owing to its altitude range, winter precipitation can occur as rain or snow, depending on the dominant atmospheric pattern.

Furthermore, traditional measurement networks using automatic snow gauges have uncertainties that can be ~20%–50%, mainly with low temperatures and strong winds (Buisán et al., 2017, 2019). To reduce the uncertainties, we did not validate snow water equivalent using only a network of snow gauges. We also used the snow-pole network as monitored by webcams and time-lapse cameras, giving 105 observation points of snow cover. Among these, 27 sites furnished snow-depth data. This has proven a valuable tool for validation of modelled snowfall events, providing a local-scale record of snow-cover evolution at the sampling points. Good fits were obtained between the modelled, webcam and snow-pole data, demonstrating that these observations have less bias than rain gauges at high altitudes (Fig. 4). Snow depth can be uneven during blizzards. To minimize this effect, we chose flat areas, sheltered from prevailing winds with no substantial vegetation cover (López-Moreno and Nogués-Bravo, 2005). The dataset improves the temporal resolution with respect to satellite products, which are frequently limited by cloud cover (Marti et al., 2016), and can reflect rapid changes in snow cover or rapid melt (Chen et al., 2012). Also, satellite platforms for snow-cover monitoring provide regional-scale data, which are very useful for analysing spatiotemporal patterns. Several studies have used passive microwave brightness temperatures to retrieve snow depth (Kilic et al., 2019; Braakmann-Folgmann and Donlon, 2019). However, the Cantabrian Mountains have frequent cloud cover, which makes continuous monitoring of the land surface impossible, especially during snowfall episodes. Combining surface observations with optical, infrared and microwave satellite data can reduce the uncertainties of each component system. Thus, in the present work, the IMS satellite product was used. This made it possible to obtain daily snow-cover data during the snowfall episodes, during which cloud cover precluded the use of other satellite platforms. The performance of IMS has been widely evaluated, especially over regions with complex topography (Li et al., 2022a; Orsolini et al., 2019). However, the grid size of WRF and IMS-NOAA does not show in detail the snow distribution in mountainous areas, where it has strong local variability caused in particular by topography and snow redistribution by wind.

The precipitation resolution of numerical weather forecast models is very sensitive to the choice of physical parameterization, especially the microphysics and PBL schemes (Miglietta et al., 2015; Patel et al., 2019).

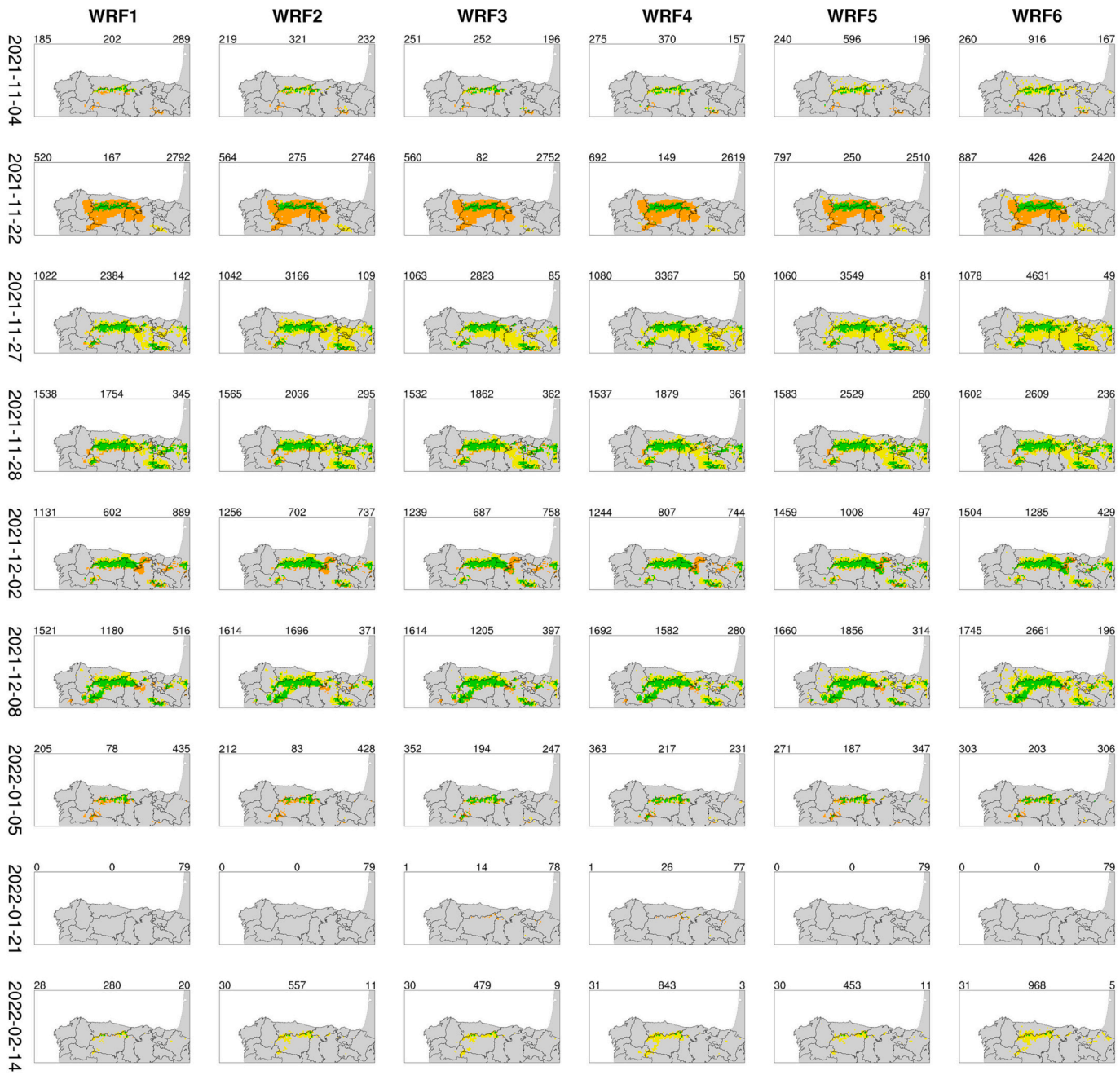

Fig. 9. Snow cover, satellite vs. WRF. Rows show study cases and columns WRF combinations. Upper numbers show number of pixels of each colour. Green (top left): WRF and satellite agree; yellow (top middle): snow cover only from WRF; orange (top right): snow cover only from satellite. (For interpretation of the references to colour in this figure legend, the reader is referred to the web version of this article.)

Thus, nine snowfall episodes in the Cantabrian mountains were simulated using WRF to test the performance of three microphysics and two PBL schemes. The model was therefore validated using several observational data sources, namely, snow gauges, snow-poles monitored by webcams, time-lapse cameras, and satellite platforms. This was done to minimize the uncertainties of each individual observational system. Once the validation databases were selected, the WRF ensemble was assessed based on three variables, liquid water equivalent, snow cover and depth.

The model performance with respect to liquid water equivalent highlights the tendency to overestimate precipitation amount with YSU PBL relative to MYNN, regardless of the microphysics used. This is consistent with previous results (Fernández-González et al., 2015; Kioutsioukis et al., 2016). One possible reason is that YSU tends to form a deeper PBL, rapidly removing inversions and increasing the convective component of precipitation, even in winter (Weisman et al., 2008; Evans et al., 2012).

Regarding microphysics, Thompson delivered better results for low altitudes and Morrison for high altitudes. Different results were found in the literature depending on the study area, the events analysed, and the validation databases used. Ghafarian (2021) evaluated a WRF multi-physics ensemble for lake-effect snow events, observing better performance with Morrison microphysics versus Thompson and Goddard. Nonetheless, in their study of a Great Salt Lake lake–effect snowstorm, McMillen and James Steenburgh (2015) found better estimation with the Thompson scheme and overprediction with Goddard and Morrison in terms of radar-based liquid equivalent precipitation. Conversely, Fernández-González et al. (2015) found that the Thompson

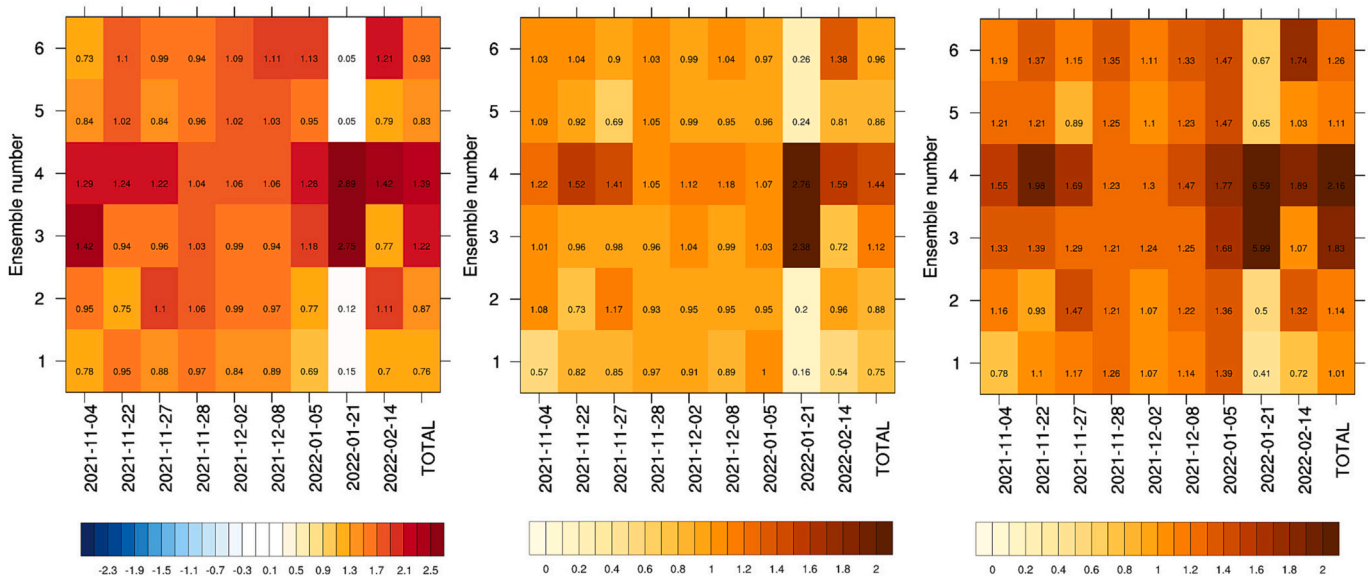

Fig. 10. Average bias (left), mean absolute error (middle), and root-mean-square error (right) for snow depth, by WRF configuration and day.

microphysics and MYJ PBL schemes better captured snow water equivalent in snowfall events over the Iberian Peninsula. However, caution is needed because of the potential loss of precipitation in the measurement systems because of blizzards (Buisán et al., 2022). Thus, the results indicated elevation as the main factor. This is a result of the underestimation of observed precipitation at altitudes >500 m a.s.l. In the selected events, precipitation collected below this level was completely liquid, but there was solid precipitation with the colder temperatures at higher altitudes. There, snow particles were readily transported by wind, especially given the isobaric gradient during most events. This caused the snow particles to impact the snow gauges horizontally rather than falling into them vertically, reducing capture. For this reason, model validation based only on liquid water equivalent may be incomplete and other variables with less uncertainty should be analysed. Furthermore, it is advisable to focus on model evaluations using other snow characteristics such as snow cover and depth. Nevertheless, most studies have concentrated on the validation of liquid water equivalent because of a lack of databases for these variables, and studies have been consequently scarce.

For snow cover validation, the models showed good performance as compared with direct observations, with CSI > 60% on most study days, although again Morrison microphysics and YSU PBL yielded the best performance. Comparisons with IMS revealed greater snow cover with Morrison microphysics and MYNN PBL and less with Goddard and YSU. Therefore, the performance of each parameterization was strongly dependent on the characteristics of each event. Thus, in the 2021-11-22 case study, there was considerable overestimation of snow cover by the IMS, in line with the results of Orsolini et al. (2019). Nevertheless, in the other case studies, the WRF output greater snow cover than the satellite product. This divergence in outcome can be related to the different atmospheric conditions of the events. The model tended to enhance moisture content for a maritime air mass and minimize it for a continental one. This is one of the potential causes of overestimation for events with northwesterly flow and underestimation with northeasterly flow. The hit rates for snow cover detection tended to increase with snow depth, providing acceptable results even in areas of small thickness (< 10 cm), where the hit rate was ~70%. This was despite being the most conflictive areas regarding correct detection of the threshold between snow cover and non-cover areas.

Finally, regarding the snow depth validation, there was substantial overestimation for all case studies and WRF configurations. Goddard microphysics produced the best outcome for all indices, whereas Thompson microphysics had the greatest overestimation. This is opposite the findings of the liquid water equivalent and snow depth validations. Opposite results were found using the WRF model coupled with the Noah land surface model (Li et al., 2022b). One of the main reasons could be the wind, which is typically strong in snowfalls of the Cantabrian Mountains because of an intense isobaric gradient. This makes observed data smaller than modelled because of compaction.

More detailed work is needed to study the behaviour of snowfall events in the Cantabrian Mountains, with augmentation of the monitoring network. In addition, global warming will substantially modify snowfall patterns in mountain ranges with low altitudes, substantially affecting the availability of water resources and the planning of winter sports.

Author contribution statement

AM and AMN. led the research, performed the analysis, prepared the Figures, and drafted the manuscript. All co-authors contributed to manuscript writing. JLS., E.G.O., AG and JS led the project and provided the funding.

Declaration of Competing Interest

The authors declare that they have no known competing financial interests or personal relationships that could have appeared to influence the work reported in this paper.

Data availability

Model data are freely available from UCAR (https://www2.mmm.ucar.edu/wrf/users/download/get_sources.html). Precipitation data, Scripts and code are available on request. Free access to live webcams is restricted to the authors due to personal data privacy, but snow cover and snow thickness data are available on request.

Acknowledgements

Funding came from projects LE240P18, LE080G19 (Consejería de Educación, Junta de Castilla y León), PID2019-108470RB-C22 and PID2019-108470RB-C21 (Ministerio de Economía y Competitividad). Adrián Melón-Nava was supported by the FPU program of the Spanish Ministerio de Universidades (FPU20/01220). The authors acknowledge

the Automatic Hydrological Information Systems (SAIH-CHEBRO, SAIH-DUERO, SAIH-CHC, SAIH-Miño-Sil), State Meteorological Agency (AEMET), and the Global Change Monitoring Programme in National Parks of the Autonomous National Parks Agency (OAPN) for the rain gauge data. The authors acknowledge funding from the GEOPAT group and Cartography Service of the Universidad de León for the monitoring network.

References

Adams-Selin, R.D., van den Heever, S.C., Johnson, R.H., 2013. Sensitivity of Bow-Echo simulation to microphysical parameterizations. Weather Forecast. 28, 1188–1209. https://doi.org/10.1175/WAF-D-12-00108.1.

AEMET (Agencia Estatal de Meteorología, España), Instituto de Meteorología (Portugal), 2011. Atlas climático ibérico: temperatura del aire y precipitación (1971–2000). https://doi.org/10.31978/784-11-002-5.

Allende Alvarez, F., 2008. Una aproximación a la caracterización climática de un sector de la montaña central cantábrica. Estud. Geogr. 69, 357–383. https://doi.org/10.3989/ESTGEOGR.0442.

Alonso-González, E., Ignacio López-Moreno, J., Gascoin, S., García-Valdecasas Ojeda, M., Sanmiguel-Vallelado, A., Navarro-Serrano, F., Revuelto, J., Ceballos, A., Esteban-Parra, M.J., Essery, R., 2018. Daily gridded datasets of snow depth and snow water equivalent for the Iberian Peninsula from 1980 to 2014. Earth Syst. Sci. Data. 10, 303–315. https://doi.org/10.5194/ESSD-10-303-2018.

Alonso-González, E., López-Moreno, J.I., Navarro-Serrano, F., Sanmiguel-Vallelado, A., Revuelto, J., Domínguez-Castro, F., Ceballos, A., 2020. Snow climatology for the mountains in the Iberian Peninsula using satellite imagery and simulations with dynamically downscaled reanalysis data. Int. J. Climatol. 40, 477–491. https://doi.org/10.1002/JOC.6223.

Alonso-González, E., Gutmann, E., Aalstad, K., Fayad, A., Bouchet, M., Gascoin, S., Alonso-González, E., Gutmann, E., Aalstad, K., Fayad, A., Bouchet, M., Gascoin, S., 2021. Snowpack dynamics in the Lebanese mountains from quasi-dynamically downscaled ERA5 reanalysis updated by assimilating remotely sensed fractional snow-covered area. HESS 25, 4455–4471. https://doi.org/10.5194/HESS-25-4455-2021.

Arslan, A.N., Tanis, C.M., Metsämäki, S., Aurela, M., Böttcher, K., Linkosalmi, M., Peltoniemi, M., 2017. Automated Webcam monitoring of fractional snow cover in Northern Boreal conditions. Geosciences 7, 55. https://doi.org/10.3390/GEOSCIENCES7030055.

Beato-Bergua, S., Poblete Piedrabuena, M.Á., Marino Alfonso, J.L., 2019. Snow avalanches, land use changes, and atmospheric warming in landscape dynamics of the Atlantic mid-mountains (Cantabrian Range, NW Spain). Appl. Geogr. 107, 38–50. https://doi.org/10.1016/j.apgeog.2019.04.007.

Blanchet, J., Davison, A.C., 2011. Spatial Modeling of Extreme Snow Depth, 5, pp. 1699–1725. https://doi.org/10.1214/11-AOAS464.

Bongio, M., Nadir Arslan, A., Melih Tanis, C., de Michele, C., 2021. Snow depth time series retrieval by time-lapse photography: Finnish and Italian case studies. Cryosphere 15, 369–387. https://doi.org/10.5194/TC-15-369-2021.

Braakmann-Folgmann, A., Donlon, C., 2019. Estimating snow depth on Arctic Sea ice using satellite microwave radiometry and a neural network. Cryosphere 13, 2421–2438. https://doi.org/10.5194/tc-13-2421-2019.

Brandes, E.A., Ikeda, K., Zhang, G., Schönhuber, M., Rasmussen, R.M., 2007. A Statistical and physical description of hydrometeor distributions in colorado snowstorms using a video disdrometer. J. Appl. Meteorol. Climatol. 46, 634–650. https://doi.org/10.1175/JAM2489.1.

Brubaker, K.L., Pinker, R.T., Deviatova, E., 2005. Evaluation and comparison of MODIS and IMS Snow-Cover estimates for the continental United States using station data. J. Hydrometeorol. 6, 1002–1017. https://doi.org/10.1175/JHM447.1.

Bryan, G.H., Morrison, H., 2012. Sensitivity of a simulated squall line to horizontal resolution and parameterization of microphysics. Mon. Weather Rev. 140, 202–225. https://doi.org/10.1175/MWR-D-11-00046.1.

Buisán, S.T., Earle, M.E., Collado, J.L., Kochendorfer, J., Alastrué, J., Wolff, M., Smith, C. D., López-Moreno, J.I., 2017. Assessment of snowfall accumulation underestimation by tipping bucket gauges in the Spanish operational network. Atmos Meas. Tech. 10, 1079–1091. https://doi.org/10.5194/AMT-10-1079-2017.

Buisán, S.T., Collado Aceituno, J.L., Alastrue Tierra, J., 2019. ¿Se mide bien la precipitación en forma de nieve?. In: Sexto Simposio Nacional de Predicción "Memorial Antonio Mestre.". Agencia Estatal de Meteorología, pp. 95–102. https://doi.org/10.31978/639-19-010-0.095.

Buisán, S.T., Serrano-Notivoli, R., Kochendorfer, J., Bello-Millán, F.J., 2022. Adjustment of Solid Precipitation during the Filomena Extreme Snowfall Event in Spain: From Observations to "True Precipitation.". Bull. Am. Meteorol. Soc. 103, E2570–E2578. https://doi.org/10.1175/BAMS-D-22-0012.1.

Chazarra-Bernabé, A., Lorenzo Mariño, B., Romero Fresneda, R., Moreno García, J.V., 2022. Evolución de los climas de Köppen en España en el periodo 1951-2020. https://doi.org/10.31978/666-22-011-4.

Chen, C., Lakhankar, T., Romanov, P., Helfrich, S., Powell, A., Khanbilvardi, R., 2012. Validation of NOAA-interactive multisensor snow and ice mapping system (IMS) by comparison with ground-based measurements over continental United States. Remote Sens. 4, 1134–1145. https://doi.org/10.3390/RS4051134.

Chen, F., Dudhia, J., 2001. Coupling an advanced land surface–Hydrology model with the Penn State–NCAR MM5 modeling system. Part I: model implementation and sensitivity. Mon. Weather Rev. 129, 569–585. https://doi.org/10.1175/1520-0493(2001)129<0569:CAALSH>2.0.CO;2.

Comin, A.N., Schumacher, V., Justino, F., 2018. Impact of different microphysical parameterizations on extreme snowfall events in the Southern Andes. Weat. Clim. Extrem. 21, 65–75. https://doi.org/10.1016/J.WACE.2018.07.001.

Corripio, J.G., López-Moreno, J.I., 2017. Analysis and predictability of the hydrological response of mountain catchments to heavy rain on snow events: a case study in the Spanish Pyrenees. Hydrology 4, 20. https://doi.org/10.3390/HYDROLOGY4020020.

Dietz, A.J., Kuenzer, C., Gessner, U., Dech, S., 2012. Remote sensing of snow – a review of available methods. Int. J. Remote Sens. 33, 4094–4134. https://doi.org/10.1080/01431161.2011.640964.

Dudhia, J., 1989. Numerical study of convection observed during the winter monsoon experiment using a mesoscale two-dimensional model. J. Atmos. Sci. 46, 3077–3107. https://doi.org/10.1175/1520-0469(1989)046<3077:NSOCOD>2.0.CO;2.

Evans, J.P., Ekström, M., Ji, F., 2012. Evaluating the performance of a WRF physics ensemble over South-East Australia. Clim. Dyn. 39, 1241–1258. https://doi.org/10.1007/S00382-011-1244-5/TABLES/2.

Fernández-González, S., Valero, F., Sánchez, J.L., Gascón, E., López, L., García-Ortega, E., Merino, A., 2015. Numerical simulations of snowfall events: Sensitivity analysis of physical parameterizations. J. Geophys. Res.-Atmos. 120 (10), 130–148. https://doi.org/10.1002/2015JD023793.

Fernández-González, S., Wang, P.K., Gascón, E., Valero, F., Sánchez, J.L., 2016. Latent cooling and microphysics effects in deep convection. Atmos. Res. 180, 189–199. https://doi.org/10.1016/J.ATMOSRES.2016.05.022.

Frei, A., Lee, S.Y., 2010. A comparison of optical-band based snow extent products during spring over North America. Remote Sens. Environ. 114, 1940–1948. https://doi.org/10.1016/J.RSE.2010.03.015.

Gallinar-Cañedo, D., Ruiz-Fernández, J., García-Hernández, C., 2022. La nieve en el Macizo de las Ubiñas (Montañas Cantábricas) y sus implicaciones geomorfológicas. Bol. Asoc. Geógr. Espan. https://doi.org/10.21138/bage.3224.

García-Hernández, C., Ruiz-Fernández, J., Sánchez-Posada, C., Pereira, S., Oliva, M., 2018. An extreme event between the Little Ice Age and the 20th century: the snow avalanche cycle of 1888 in the Asturian Massif (Northern Spain). Cuader. Investig. Geogr. 44, 187–212. https://doi.org/10.18172/CIG.3386.

Gerber, F., Besic, N., Sharma, V., Mott, R., Daniels, M., Gabella, M., Berne, A., Germann, U., Lehning, M., 2018. Spatial Variability of Snow Precipitation and Accumulation in COSMO-WRF Simulations and Radar Estimations Over Complex Terrain. https://doi.org/10.5194/tc-2018-50.

Ghafarian, P., 2021. Impact of physical parameterizations on simulation of the Caspian Sea lake-effect snow. Dyn. Atmos. Oceans 94, 101219. https://doi.org/10.1016/J.DYNATMOCE.2021.101219.

González Trueba, J.J., Serrano Cañadas, E., 2010. Snow in the Picos de Europa: geomorphological and environmental implications. Cuader. Investig. Geogr. 36, 61–84. https://doi.org/10.18172/CIG.1238.

Grossi, G., Lendvai, A., Peretti, G., Ranzi, R., 2017. Snow precipitation measured by Gauges: systematic error estimation and data series correction in the Central Italian Alps. Water 9, 461. https://doi.org/10.3390/W9070461.

Gupta, H.V., Kling, H., Yilmaz, K.K., Martinez, G.F., 2009. Decomposition of the mean squared error and NSE performance criteria: implications for improving hydrological modelling. J. Hydrol. 377, 80–91. https://doi.org/10.1016/J.JHYDROL.2009.08.003.

Hammer, H.L., 2018. Statistical models for short- and long-term forecasts of snow depth. J. Appl. Stat. 45, 1133–1156. https://doi.org/10.1080/02664763.2017.1357683.

He, Q., Zuo, Z., Zhang, Renhe, Yang, S., Wang, W., Zhang, Ruonan, Riddle, E.E., 2016. Prediction skill and predictability of Eurasian snow cover fraction in the NCEP climate Forecast System version 2 reforecasts. Int. J. Climatol. 36, 4071–4084. https://doi.org/10.1002/JOC.4618.

Helfrich, S.R., McNamara, D., Ramsay, B.H., Baldwin, T., Kasheta, T., 2007. Enhancements to, and forthcoming developments in the Interactive Multisensor Snow and Ice Mapping System (IMS). Hydrol. Process. 21, 1576–1586. https://doi.org/10.1002/HYP.6720.

Heymsfield, A.J., van Zadelhoff, G.J., Donovan, D.P., Fabry, F., Hogan, R.J., Illingworth, A.J., 2007. Refinements to ice particle mass dimensional and terminal velocity relationships for ice clouds. Part II: Evaluation and parameterizations of ensemble ice particle sedimentation velocities. J. Atmos. Sci. 64, 1068–1088. https://doi.org/10.1175/JAS3900.1.

Hong, S.Y., Noh, Y., Dudhia, J., 2006. A new vertical diffusion package with an explicit treatment of entrainment processes. Mon. Weather Rev. 134, 2318–2341. https://doi.org/10.1175/MWR3199.1.

Janjić, Z.I., 1994. The step-mountain eta coordinate model: further developments of the convection, viscous sublayer, and turbulence closure schemes. Mon. Weather Rev. 122, 927–945. https://doi.org/10.1175/1520-0493(1994)122<0927:TSMECM>2.0.CO;2.

Kain, J.S., 2004. The Kain–Fritsch convective parameterization: an update. J. Appl. Meteorol. Climatol. 43, 170–181. https://doi.org/10.1175/1520-0450(2004)043.

Kilic, L., Tage Tonboe, R., Prigent, C., Heygster, G., Kilic, L., Tage Tonboe, R., Prigent, C., Heygster, G., 2019. Estimating the snow depth, the snow-ice interface temperature, and the effective temperature of Arctic Sea ice using Advanced Microwave Scanning Radiometer 2 and ice mass balance buoy data. Cryosphere 13, 1283–1296. https://doi.org/10.5194/TC-13-1283-2019.

Kioutsioukis, I., de Meij, A., Jakobs, H., Katragkou, E., Vinuesa, J.F., Kazantzidis, A., 2016. High resolution WRF ensemble forecasting for irrigation: multi-variable evaluation. Atmos. Res. 167, 156–174. https://doi.org/10.1016/J.ATMOSRES.2015.07.015.

Kling, H., Fuchs, M., Paulin, M., 2012. Runoff conditions in the upper Danube basin under an ensemble of climate change scenarios. J. Hydrol. 424–425, 264–277. https://doi.org/10.1016/J.JHYDROL.2012.01.011.

Lastrada, E., Garzón-Roca, J., Cobos, G., Torrijo, F.J., Ignacio, J., Moreno, L., Polo, M.-J., Gascoin, S., 2021. A decrease in the regulatory effect of snow-related phenomena in Spanish Mountain areas due to climate change. Water 13, 1550. https://doi.org/10.3390/W13111550.

Lee, J., Lee, S.-M., Lee, S.-J., 2022. Ground- and satellite-based evaluation of WRF snowfall prediction. SOLA 18, 173–180. https://doi.org/10.2151/SOLA.2022-028.

Li, Q., Yang, T., Li, L., 2022a. Evaluation of snow depth and snow cover represented by multiple datasets over the Tianshan Mountains: remote sensing, reanalysis, and simulation. Int. J. Climatol. 42, 4223–4239. https://doi.org/10.1002/JOC.7459.

Li, Q., Yang, T., Li, L., Li, Q., Yang, T., Li, L., 2022b. Quantitative assessment of the parameterization sensitivity of the WRF/Noah-MP model of snow dynamics in the Tianshan Mountains, Central Asia. Atmos. Res. 277, 106310 https://doi.org/10.1016/J.ATMOSRES.2022.106310.

Li, X., Tao, W.K., Khain, A.P., Simpson, J., Johnson, D.E., 2009a. Sensitivity of a cloud-resolving model to bulk and explicit bin microphysical schemes. Part II: cloud microphysics and storm dynamics interactions. J. Atmos. Sci. 66, 22–40. https://doi.org/10.1175/2008JAS2647.1.

Li, X., Tao, W.K., Khain, A.P., Simpson, J., Johnson, D.E., 2009b. Sensitivity of a cloud-resolving model to bulk and explicit bin microphysical schemes. Part I: comparisons. J. Atmos. Sci. 66, 3–21. https://doi.org/10.1175/2008JAS2646.1.

Li, X., Tao, W.K., Matsui, T., Liu, C., Masunaga, H., 2010. Improving a spectral bin microphysical scheme using TRMM satellite observations. Q. J. R. Meteorol. Soc. 136, 382–399. https://doi.org/10.1002/QJ.569.

Li, Y., Chen, Y., Li, Z., 2019. Developing daily cloud-free snow composite products from MODIS and IMS for the Tienshan Mountains. Earth Space Sci. 6, 266–275. https://doi.org/10.1029/2018EA000460.

Liu, C., Moncrieff, M.W., 2007. Sensitivity of cloud-resolving simulations of warm-season convection to cloud microphysics parameterizations. Mon. Weather Rev. 135, 2854–2868. https://doi.org/10.1175/MWR3437.1.

Liu, L., Ma, Y., Menenti, M., Zhang, X., Ma, W., 2018. Evaluation of WRF modeling in relation to different land surface schemes and initial and boundary conditions: a snow event simulation over the Tibetan Plateau. J. Geophys. Res.-Atmos. 124, 209–226. https://doi.org/10.1029/2018JD029208.

López-Moreno, J.I., Nogués-Bravo, D., 2005. A generalized additive model for the spatial distribution of snowpack in the Spanish Pyrenees. Hydrol. Process. 19, 3167–3176. https://doi.org/10.1002/HYP.5840.

Mankin, J.S., Viviroli, D., Singh, D., Hoekstra, A.Y., Diffenbaugh, N.S., 2015. The potential for snow to supply human water demand in the present and future. Environ. Res. Lett. 10 https://doi.org/10.1088/1748-9326/10/11/114016.

Marti, R., Gascoin, S., Berthier, E., de Pinel, M., Houet, T., Laffly, D., 2016. Mapping snow depth in open alpine terrain from stereo satellite imagery. Cryosphere 10, 1361–1380. https://doi.org/10.5194/TC-10-1361-2016.

Masuda, M., Yatagai, A., Kamiguchi, K., Tanaka, K., 2019. Daily adjustment for wind-induced precipitation undercatch of daily gridded precipitation in Japan. Earth Space Sci. 6, 1469–1479. https://doi.org/10.1029/2019EA000659.

McMillen, J.D., James Steenburgh, W., 2015. Impact of microphysics parameterizations on simulations of the 27 October 2010 Great Salt Lake–effect snowstorm. Weather Forecast. 30, 136–152. https://doi.org/10.1175/WAF-D-14-00060.1.

Mellor, G.L., Yamada, T., 1974. A Hierarchy of turbulence closure models for planetary boundary layers. J. Atmos. Sci. 31, 1791–1806. https://doi.org/10.1175/1520-0469(1974)031<1791:AHOTCM>2.0.CO;2.

Mellor, G.L., Yamada, T., 1982. Development of a turbulence closure model for geophysical fluid problems. Rev. Geophys. 20, 851–875. https://doi.org/10.1029/RG020I004P00851.

Melón-Nava, A., Santos-González, J., María Redondo-Vega, J., Blanca González-Gutiérrez, R., Gómez-Villar, A., 2022. Factors influencing the ground thermal regime in a mid-latitude glacial cirque (Hoyo Empedrado, Cantabrian Mountains, 2006–2020). Catena 212, 106110. https://doi.org/10.1016/J.CATENA.2022.106110.

Merino, A., Fernández, S., Hermida, L., López, L., Sánchez, J.L., García-Ortega, E., Gascón, E., 2014. Snowfall in the Northwest Iberian Peninsula: synoptic circulation patterns and their influence on snow day trends. Sci. World J. 2014 https://doi.org/10.1155/2014/480275.

Merino, A., García-Ortega, E., Navarro, A., Fernández-González, S., Tapiador, F.J., Sánchez, J.L., 2021. Evaluation of gridded rain-gauge-based precipitation datasets: Impact of station density, spatial resolution, altitude gradient and climate. Int. J. Climatol. 41, 3027–3043. https://doi.org/10.1002/JOC.7003.

Miglietta, M.M., Mastrangelo, D., Conte, D., 2015. Influence of physics parameterization schemes on the simulation of a tropical-like cyclone in the Mediterranean Sea. Atmos. Res. C 360–375. https://doi.org/10.1016/J.ATMOSRES.2014.09.008.

Milbrandt, J.A., Morrison, H., 2016. Parameterization of cloud microphysics based on the prediction of bulk ice particle properties. Part III: introduction of multiple free categories. J. Atmos. Sci. 73, 975–995. https://doi.org/10.1175/JAS-D-15-0204.1.

Mlawer, E.J., Taubman, S.J., Brown, P.D., Iacono, M.J., Clough, S.A., 1997. Radiative transfer for inhomogeneous atmospheres: RRTM, a validated correlated-k model for the longwave. J. Geophys. Res.-Atmos. 102, 16663–16682. https://doi.org/10.1029/97JD00237.

Molthan, A.L., Colle, B.A., 2012. Comparisons of single- and double-moment microphysics schemes in the simulation of a synoptic-scale snowfall event. Mon. Weather Rev. 140, 2982–3002. https://doi.org/10.1175/MWR-D-11-00292.1.

Morrison, H., Milbrandt, J.A., 2015. Parameterization of cloud microphysics based on the prediction of bulk ice particle properties. Part I: scheme description and idealized tests. J. Atmos. Sci. 72, 287–311. https://doi.org/10.1175/JAS-D-14-0065.1.

Musselman, K.N., Lehner, F., Ikeda, K., Clark, M.P., Prein, A.F., ChangHai, L., Barlage, M., Rasmussen, R., 2018. Projected increases and shifts in rain-on-snow flood risk over western North America. Nat. Clim. Chang. 8, 808–812. https://doi.org/10.1038/s41558-018-0236-4.

Nakanishi, M., Niino, H., 2006. An improved Mellor–Yamada Level-3 Model: its numerical stability and application to a regional prediction of advection fog. Bound.-Layer Meteorol. 119, 397–407. https://doi.org/10.1007/S10546-005-9030-8.

Nitu, R., Roulet, Y.-A., Wolff, M., Earle, M.E., Reverdin, A., Smith, C.D., Kochendorfer, J., Morin, S., Rasmussen, R., Wong, K., Alastrué Tierra, J.J., Arnold, L., Baker, B., Buisán Sanz, S.T., Collado Aceituno, J.L., Colli, M., Collins, B., Gaydos, A., Hannula, H.-R., Hoover, J., Joe, P., Kontu, A., Laine, T., Lanza, L., Lanzinger, E., Lee, G., Lejeune, Y., Leppänen, L., Mekis, E., Panel, J.-M., Poikonen, A., Ryu, S., Sabatini, F., Thériault, J.M., Yang, D., Genthon, C., van den Heuvel, F., Hirasawa, N., Konishi, H., Motoyoshi, H., Nakai, S., Nishimura, K., Senese, A., Yamashita, K., 2019. WMO Solid Precipitation Intercomparison Experiment (SPICE) (2012–2015). http://hdl.handle.net/20.500.11765/10839.

Noh, Y., Cheon, W.G., Hong, S.Y., Raasch, S., 2003. Improvement of the K-profile Model for the Planetary Boundary Layer based on large Eddy simulation data. Bound.-Layer Meteorol. 107 (2), 401–427. https://doi.org/10.1023/A:1022146015946.

Nykänen, M.L., Peltola, H., Quine, C., Kellomäki, S., Broadgate, M., 1997. Factors affecting snow damage of trees with particular reference to European conditions. Silva Fennica 31, 193–213. https://doi.org/10.14214/SF.A8519.

Olson, J.B., Kenyon, J.S., Angevine, Wayne A., Brown, J.M., Pagowski, M., Sušelj, K., 2019. A description of the MYNN-EDMF scheme and the coupling to other components in WRF–ARW. NOAA Tech. Memorand. OAR GSD 61. https://doi.org/10.25923/N9WM-BE49.

Orsolini, Y., Wegmann, M., Dutra, E., Liu, B., Balsamo, G., Yang, K., de Rosnay, P., Zhu, C., Wang, W., Senan, R., Arduini, G., 2019. Evaluation of snow depth and snow cover over the Tibetan Plateau in global reanalyses using in situ and satellite remote sensing observations. Cryosphere 13, 2221–2239. https://doi.org/10.5194/TC-13-2221-2019.

Ortega-Villazán, M.T., Morales-Rodríguez, C.G., 2015. El clima de la Cordillera Cantábrica castellano-leonesa: diversidad, contrastes y cambios. Investig. Geogr. 0, 45–67. https://doi.org/10.14198/INGEO2015.63.04.

Patel, P., Ghosh, S., Kaginalkar, A., Islam, S., Karmakar, S., 2019. Performance evaluation of WRF for extreme flood forecasts in a coastal urban environment. Atmos. Res. 223, 39–48. https://doi.org/10.1016/J.ATMOSRES.2019.03.005.

Piazzi, G., Tanis, C.M., Kuter, S., Simsek, B., Puca, S., Toniazzo, A., Takala, M., Akyürek, Z., Gabellani, S., Arslan, A.N., 2019. Cross-country assessment of H-SAF Snow products by Sentinel-2 imagery validated against in-situ observations and webcam photography. Geosciences 9, 129. https://doi.org/10.3390/GEOSCIENCES9030129.

Pisabarro, A., Pellitero, R., Serrano, E., Gómez-Lende, M., González-Trueba, J.J., Pisabarro, A., Pellitero, R., Serrano, E., Gómez-Lende, M., González-Trueba, J.J., 2017. Ground temperatures, landforms and processes in an Atlantic mountain. Cantabrian Mountains (Northern Spain). Catena 149, 623–636. https://doi.org/10.1016/J.CATENA.2016.07.051.

Pisabarro, A., Pellitero, R., Serrano, E., Lopez-Moreno, J.I., Pisabarro, A., Pellitero, R., Serrano, E., Lopez-Moreno, J.I., 2019. Impacts of land abandonment and climate variability on runoff generation and sediment transport in the Pisuerga headwaters (Cantabrian Mountains, Spain). Geogr. Ann. Ser. A: Phys. Geogr. 101, 211–224. https://doi.org/10.1080/04353676.2019.1591042.

Pons, M.R., San-Martín, D., Herrera, S., Gutiérrez, J.M., 2010. Snow trends in Northern Spain: analysis and simulation with statistical downscaling methods. Int. J. Climatol. 30, 1795–1806. https://doi.org/10.1002/JOC.2016.

Portenier, C., Hüsler, F., Härer, S., Wunderle, S., 2020. Towards a webcam-based snow cover monitoring network: Methodology and evaluation. Cryosphere 14, 1409–1423. https://doi.org/10.5194/TC-14-1409-2020.

Pulliainen, J., Luojus, K., Derksen, C., Mudryk, L., Lemmetyinen, J., Salminen, M., Ikonen, J., Takala, M., Cohen, J., Smolander, T., Norberg, J., 2020. Patterns and trends of Northern Hemisphere snow mass from 1980 to 2018. Nature 581, 294–298. https://doi.org/10.1038/S41586-020-2258-0.

Ramsay, B.H., 1998. The interactive multisensor snow and ice mapping system. Hydrol. Process. 12, 1537–1546. https://doi.org/10.1002/(SICI)1099-1085(199808/09)12:10/11<1537::AID-HYP679>3.0.CO;2-A.

Raparelli, E., Tuccella, P., Colaiuda, V., Marzano, F.S., 2023. Snow cover prediction in the Italian central Apennines using weather forecast and land surface numerical models. Cryosphere 17, 519–538. https://doi.org/10.5194/tc-17-519-2023.

Rasmussen, R., Baker, B., Kochendorfer, J., Meyers, T., Landolt, S., Fischer, A.P., Black, J., Thériault, J.M., Kucera, P., Gochis, D., Smith, C., Nitu, R., Hall, M., Ikeda, K., Gutmann, E., 2012. How well are we measuring snow: the NOAA/FAA/NCAR winter precipitation test bed. Bull. Am. Meteorol. Soc. 93, 811–829. https://doi.org/10.1175/BAMS-D-11-00052.1.

Rudisill, W., Flores, A., McNamara, J., 2021. The impact of initial snow conditions on the numerical weather simulation of a Northern Rockies atmospheric river. J. Hydrometeorol. 22, 155–167. https://doi.org/10.1175/JHM-D-20-0018.1.

Santos-González, J., Redondo Vega, J.M., Gómez Villar, A., González Gutiérrez, R.B., 2010a. Avalanches in the Alto Sil (Western Cantabrian Mountain, Spain). Cuader. Investig. Geogr. 36, 7–26. https://doi.org/10.18172/CIG.1224.

Santos-González, J., Redondo Vega, J.M., Gómez Villar, A., González Gutiérrez, R.B., 2010b. Current dynamic of nivation hollows in the Alto Sil (Cantabrian Mountain). Cuader. Investig. Geogr. 36, 87–106. https://doi.org/10.18172/CIG.1229.

Scherrer, S.C., Wüthrich, C., Croci-Maspoli, M., Weingartner, R., Appenzeller, C., 2013. Snow variability in the Swiss Alps 1864–2009. Int. J. Climatol. 33, 3162–3173. https://doi.org/10.1002/JOC.3653.

Schwartz, C.S., Kain, J.S., Weiss, S.J., Xue, M., Bright, D.R., Kong, F., Thomas, K.W., Levit, J.J., Coniglio, M.C., Wandishin, M.S., 2010. Toward improved convection-allowing ensembles: model physics sensitivities and optimizing probabilistic guidance with small ensemble membership. Weather Forecast. 25, 263–280. https://doi.org/10.1175/2009WAF2222267.1.

Serrano, E., Gómez-Lende, M., Pellitero, R., González-Trueba, J.J., 2015. Deglaciation in the Cantabrian Mountains: pattern and evolution. Cuader. Investig. Geogr. 41, 389–408. https://doi.org/10.18172/CIG.2716.

Skamarock, W.C., Klemp, J.B., 2008. A time-split non-hydrostatic atmospheric model for weather research and forecasting applications. J. Comput. Phys. 227, 3465–3485. https://doi.org/10.1016/J.JCP.2007.01.037.

Somos-Valenzuela, M., Manquehual-Cheuque, F., 2020. Evaluating Multiple WRF Configurations and Forcing over the Northern Patagonian Icecap (NPI) and Baker River Basin. Atmosphere 11, 815. https://doi.org/10.3390/ATMOS11080815.

Tanis, C.M., Arslan, A.N., Rautiainen, M., 2020. Near real time monitoring of snow cover using webcam imagery. EGU2020. https://doi.org/10.5194/EGUSPHERE-EGU2020-22347.

Tao, W.K., Anderson, D., Chern, J., Entin, J., Hou, A., Houser, P., Kakar, R., Lang, S., Lau, W., Peters-Lidard, C., Li, X., Matsui, T., Rienecker, M., Schoeberl, M.R., Shen, B. W., Shi, J.J., Zeng, X., 2009. The Goddard multi-scale modeling system with unified physics. Ann. Geophys. 27, 3055–3064. https://doi.org/10.5194/ANGEO-27-3055-2009.

Tao, W.K., Wu, D., Lang, S., Chern, J.D., Peters-Lidard, C., Fridlind, A., Matsui, T., 2016. High-resolution NU-WRF simulations of a deep convective-precipitation system during MC3E: further improvements and comparisons between Goddard microphysics schemes and observations. J. Geophys. Res.-Atmos. 121, 1278–1305. https://doi.org/10.1002/2015JD023986.

Thompson, G., Rasmussen, R.M., Manning, K., 2004. Explicit forecasts of winter precipitation using an improved bulk microphysics scheme. Part I: Description and sensitivity analysis. Mon. Weather Rev. 519–542.

Thompson, G., Field, P.R., Rasmussen, R.M., Hall, W.D., 2008. Explicit forecasts of winter precipitation using an improved bulk microphysics scheme. Part II: implementation of a new snow parameterization. Mon. Weather Rev. 136, 5095–5115. https://doi.org/10.1175/2008MWR2387.1.

Vignon Besic, N., Jullien, N., Gehring, J., Berne, A., 2019. Microphysics of Snowfall over Coastal East Antarctica simulated by Polar WRF and Observed by Radar. J. Geophys. Res.-Atmos. 124, 11452–11476. https://doi.org/10.1029/2019JD031028.

Viviroli, D., Kummu, M., Meybeck, M., Kallio, M., Wada, Y., 2020. Increasing dependence of lowland populations on mountain water resources. Nature Sustain. 11 (3), 917–928. https://doi.org/10.1038/s41893-020-0559-9.

Wang, P.K., Ji, W., 2000. Collision efficiencies of ice crystals at low-intermediate reynolds numbers colliding with supercooled cloud droplets: a numerical study. J. Atmos. Sci. 57, 1001–1009. https://doi.org/10.1175/1520-0469(2000)057.

Weisman, M.L., Davis, C., Wang, W., Manning, K.W., Klemp, J.B., 2008. Experiences with 0–36-h Explicit Convective forecasts with the WRF-ARW Model. Weather Forecast. 23, 407–437. https://doi.org/10.1175/2007WAF2007005.1.